# Catalysis Science & Technology

Accepted Manuscript






ROYAL SOCIETY OF CHEMISTRY

www.rsc.org/catalysis

Journal Name

ARTICLE

# Comparative study of bioethanol transformation catalyzed by Ru or Pt nanoparticles supported on KL zeolite

Received 00th January 20xx,
Accepted 00th January 20xx

DOI: 10.1039/x0xx00000x

www.rsc.org/

M. Almohalla,[a] E. Gallegos-Suarez,[a,b] A. Arcoya,[b,c] I. Rodríguez-Ramos,[b,c] and A. Guerrero-Ruiz[a,c]

The catalytic properties of two noble metals, Pt and Ru, supported on KL zeolite were investigated in the selective transformation of bioethanol. In aiming to have an increased basicity of the catalyst, a KL zeolite modified by the addition of Ba was also used as support for Pt catalyst. For comparative purposes Ru supported on hydrophobic high surface area graphite (HSAG) was also prepared. The catalytic tests were conducted in a fixed bed flow reactor feeding ethanol in an inert gas, either pure ethanol vapor or a mixture of 10%water/90%ethanol, and working at low conversions to assure kinetic conditions. All the catalysts have relatively stable catalytic performances at less up to 6 hours on stream with both reactant feedings. In general the catalytic activities of Pt based catalysts, given as turn-over-frequencies, were one order of magnitude higher than those obtained over Ru catalysts. It was also demonstrated that the nature of the supported metal nanoparticles (Ru vs. Pt) significantly affects the product selectivities. So when comparing Pt/KL and Ru/KL, methane and carbon monoxide byproducts are mainly produced on the former, indicating that degradation of the primary product acetaldehyde by decarbonylation is higher on Pt catalysts. In the case of ruthenium nanoparticles, acetaldehyde is the predominant product. Finally by the comparison of Ru supported on KL zeolite and on HSAG revealed that, in the second case, ethylene is the principal byproduct and that in some extension this ethylene can be hydrogenated to ethane, provably spending hydrogen generated in the acetaldehyde formation. DRIFTS experiments were also conducted to identify the adsorbed intermediate species present under reaction conditions on the different catalysts. All the selectivity differences have been rationalized using appropriate reaction pathways, and it is inferred that the variation of the chosen metal-support system is decisive to obtain a given reaction product.

## Introduction

The use of light alcohols, such as methanol or ethanol, for producing energy is an attractive option in terms of sustainability and low environmental impact.[1] The manufacture of bioethanol from cellulosic residues currently exceeds 50 million tons per year and it is expected that this production is increased all over the world in the next decades. Taking into account the large availability of ethanol in the future, its use in the preparation of automotive fuels, as well as feedstock for the chemical industry, can be foreseen.[2] In recent years the chemistry of ethanol has attracted increasing attention for producing different chemicals. The more feasible transformations of ethanol by heterogeneous catalysts are those yielding ethylene or acetaldehyde. In the first case ethanol is transformed by dehydration over acid surface sites[3-6] while acetaldehyde is obtained by dehydrogenation over basic[7] or metallic catalysts.[8] Acetaldehyde is an important chemical because it could be used as a raw material for the production of acetic acid, acetic anhydride, ethyl acetate, butyl aldehyde, crotonaldehyde, pyridine, peracetic acid, vinylacetate and many other products.[9] Chang et al. reported that copper catalysts supported on rice husk ash displayed high catalytic activity and selectivity towards dehydrogenation products.[8] Much attention has been focused on preparing catalysts with acidic or basic sites in order to promote dehydration or dehydrogenation reactions, respectively.[10-13] In this sense the use of zeolites YZ and ZSM5 ion exchanged with alkaline cations has demonstrated the positive effect of basicity on the selectivity towards dehydrogenation products, in such a way that the lower electronegativity of the countercation the higher the selectivity towards dehydrogenation activity,[14-16] because basic sites weaken the OH bond of ethanol adsorbed on the zeolite.[17] Likewise, activity of these zeolites is enhanced by incorporation of a metallic component[18] giving rise to a bifunctional catalyst.

[a] Dpto. Química Inorgánica y Técnica, UNED, Paseo Senda del Rey 9, 28040-Madrid, Spain.
[b] Instituto de Catálisis y Petroleoquímica, CSIC, C/Marie Curie 2, 28049-Madrid, Spain.
[c] Grupo de Diseño y Aplicación de Catalizadores Heterogéneos, Unidad Asociada UNED-CSIC (ICP), Spain.

† Footnotes relating to the title and/or authors should appear here.
Electronic Supplementary Information (ESI) available: [details of any supplementary information available should be included here]. See DOI: 10.1039/x0xx00000x

KL is a basic synthetic zeolite whose structure consists of a tri-dimensional system with parallel channels constituted by cages of 0.48 nm x 1.24 nm x 1.07 nm, connected by windows of 12-membered rings of 0.71 nm diameter.[19] Basicity of this zeolite arises from the low electronegativity of $K^+$ as countercation and mainly from the particular location of the electron-donor oxygen atoms in its characteristic framework structure. Catalysts of platinum supported on KL zeolite have been reported to be highly active and selective in the dehydrocyclization of light alkanes due, in part, to the singular ability of the zeolite to stabilize electron rich metal particles inside the channels.[20-22] Metal catalysts supported on KL have been also used in the selective hydrogenation of α,β-unsaturated aldehydes[23,24] but, to our knowledge it does not have been used in ethanol dehydrogenation reaction, in spite of its basic character. In this work we study comparatively the catalytic properties of two noble metals, Pt and Ru, supported over one commercial KL zeolite and over KL zeolite modified with barium (BaKL) in the selective transformation of bioethanol. The addition of Ba can change the basicity properties of KL zeolite and can contribute to an electron-enrichment of the Pt particles[25]. Since KL is a non-acidic zeolite it can be expected that reactions involving acid sites are minimized, so we mainly determine the reaction pathways involved in the acetaldehyde formation and decompostion over the metal nanoparticles. In order to interpret and to explain the catalytic performances of these bifunctional catalysts, they were characterized by X-ray diffraction (XRD), temperature-programmed reduction (TPR), transmission electron microscopy (TEM) and CO chemisorption. Furthermore the surface species generated on these catalysts during ethanol decomposition were investigated, under reaction conditions, by in situ diffuse reflectance infrared Fourier transform spectroscopy (DRIFTS).

## Experimental

### Catalyst preparation

Two catalysts containing 1 wt% of platinum were prepared by incipient wetness impregnation employing two different supports. One of them was the as-received commercial KL-zeolite (Union Carbide, SK-45, $K_9Al_9Si_{27}O_{72}$ in atoms per unit cell) only previously calcined at 873 K for 3 h. The other support was a portion of that material modified with barium. This later was prepared by incipient wetness impregnation of the zeolite with 5 wt% of Ba using a barium nitrate aqueous solution, after that the sample was dried overnight and calcined at 873 K for 3h. The surface areas of KL and BaKL were 245 and 105 $m^2/g$ respectively. Both supports were impregnated with an aqueous solution of tetraammine platinum (IV) hydroxide. After drying at 393 K overnight, the metallic precursor was decomposed by calcination at 573 K under pure oxygen stream. Before use the catalysts were reduced at 673 K under hydrogen flow for 2 h and then cooled down to the reaction temperature under inert flow. These catalysts were called Pt/KL and Pt/BaKL, respectively.

Ruthenium catalysts were prepared by incipient wetness impregnation employing aqueous solutions of ruthenium (III) nitrosyl nitrate when using both KL-zeolite and high surface area graphite (HSAG) supports. The surface area of this HSAG is 400 $m^2/g$. The loading of Ru in both samples is 2 wt%.

### Catalyst characterization

Temperature-programmed reduction (TPR) experiments were carried out in dynamic regime, employing a U-shape quartz reactor. The TPR profiles were registered heating the samples from room temperature to 973 K at 2.5 K $min^{-1}$ under a flow of 10% $H_2$/He mixture (20 mL/min). The effluent gas of the reactor was analyzed in a gas chromatograph provided with an automatic injection valve, a thermal conductivity detector and a Porapack Q column.

CO chemisorptions were performed in a volumetric glass vacuum-dosing apparatus connected to a heat-flow microcalorimeter (Setaram C-80 II) operated isothermally at 330 K. This device has been described in detail elsewhere.[26] For these experiments the catalyst samples were first reduced in situ under hydrogen flow at 673 K for 2 h, outgassed overnight at the same temperature and cooled down to 330 K. Successive doses of the probe gas were introduced into the system to titrate the metal surface of the sample. Both calorimetric and volumetric data were stored and evaluated by microcomputer processing. Metal dispersion ($D_{CO}$) was calculated from the total CO uptake at the monolayer ($N_{CO}$), considered to be attained when the evolved adsorption heat falls to the physisorption field (40 kJ/mol), and assuming an adsorption stoichiometry of CO/Pt and CO/Ru of unity.[27] The average metal particle sizes were calculated from the dispersion values, assuming spherical model of particle, using the equations: d(nm)=1.03/D and d(nm)=1.32/D for platinum and ruthenium, respectively.[28]

Specific surface areas were calculated using the BET method from nitrogen adsorption isotherms, recorded at the temperature of liquid nitrogen on a Micromeritics ASAP 2010 apparatus.

The TEM analysis was made using a JEOL 2100 F field emission gun electron microscope operated at 200 kV. The TEM specimens were prepared by dispersing a small catalyst amount in ethanol and placing one drop of the dispersion on a lacey carbon film coated copper grid (3.0 mm, 200 mesh, Aname manufacturer) and allowing the solvent to evaporate. Over 200 individual metal particles were counted for each catalyst and the surface–weighted metal particle diameter ds was calculated using the following equation (1)

$$d=\sum_i n_i d_i^3 / \sum_i n_i d_i^2 \quad (1)$$

where $n_i$ is the number of particles with diameter $d_i$.

### In situ DRIFT spectroscopy studies

In situ diffuse reflectance infrared Fourier transform spectroscopy (DRIFTS) was applied to the study of the behavior of catalysts in the transformation of ethanol. DRIFTS spectra were collected by using a VARIAN 670 spectrometer equipped with a MCT detector and a Harrick environmental cell. Before

the adsorption of reactant, the catalyst sample was reduced under $H_2$ stream (20 mL/min) at 673 K for 1 h, and then cooled down to 373 K in Ar. At this temperature a spectrum of the bare sample was obtained. The reaction was carried out by admitting a flow (20 mL/min) of Ethanol/Argon (molar ratio 2/18) to the DRIFT cell. This reaction mixture was adjusted using a thermostated saturator at 298 K and a calibrated flowmeter. The cell temperature was raised from 373 K to 723 K in several successive steps, and at each stabilized reaction temperature the spectra were recorded. All spectra measured in reflectance were subsequently converted via Kubelka–Munk transformation.

#### Catalytic activity measurements

The catalytic activity of the samples in the decomposition of ethanol was studied in the gas phase, at atmospheric pressure and several different temperatures, in a PID Microactivity apparatus using a glass made fixed bed tubular microreactor (i.d. 9 mm). The mass of catalyst was adjusted in each experiment in order to attain isoconversion levels in the range 5-15 %.

In a typical experiment, the catalyst sieved to particle grain between 0.5 and 1 mm was diluted with solid-glass beads in order to avoid local heating effect. Ethanol (either pure or containing water at 10%) was charged through a micro-pump, using helium as carrier gas. The total gas flow (He plus vaporized ethanol) was kept constant at 20.66 mL/min. The composition of the reactor effluent was analyzed using a gas chromatograph (Varian CP-3800) equipped with a Porapak Q column and two detectors (FID and TCD). By this TCD detector the formation of CO and $CO_2$ was analysed. Blank experiments were done to verify the absence of catalytic activity in the conditions used in this study, either with the empty reactor or filled with the glass beads. To avoid the condensation of reactant or products, all the pipelines were thermostated at 423 K. The ethanol conversion was defined as the ratio of the amount of ethanol converted to the amount of ethanol fed to the reactor. Selectivity towards a product i ($S_i$) is defined as the number of ethanol molecules converted into i per 100 molecules of ethanol transformed.

## Results and discussion

#### Catalysts characterization

Table 1 summarizes metal loading, metal dispersion ($D_{CO}$) and average metal particle size of the catalysts ($d_{CO}$) obtained from both the CO chemisorption measurements, as well as the particle sizes determined from TEM ($d_{TEM}$). Metal dispersion values differ from one catalyst to others. Platinum is well dispersed (42%) in Pt/KL sample, but it is noticeable the negative effect of barium on the metal dispersion of Pt/BaKL (25%). Furthermore the BET surface area of BaKL support, 105 $m^2/g$, is significantly lower than that of KL, 245 $m^2/g$, which could indicate that Ba blocks partially the zeolite channels. Thus, assuming that the basic sites of the zeolite inside the channels can act as anchoring sites for $Pt(NH_3)_4^{2+}$ cations of the metal precursor, the impeded access of the Pt precursor into the channels could explain that metal dispersion for Pt/BaKL is lower than for Pt/KL. On the other hand, the average metal particle sizes for all the catalysts (Pt or Ru) are larger than the dimensions of the zeolite cages (0.48 x 1.24x 0.71 nm). Thus at least part of the metal particles would be located at the outer surface of the zeolite, i.e. in the intercrystalline spaces. It was previously confirmed by XRD that incorporation of Ba does not affect the structural stability of the KL framework.

Table 1. Nomenclature and characterization of the catalysts.

| Catalyst | Precursors | Metal (wt%) | $\mu mol_{CO}/g_{cat}$ | $D_{CO}$ (%) | $d_{co}$(nm) | $d_{TEM}$(nm) |
|---|---|---|---|---|---|---|
| Pt/KL | $Pt(NH_3)_4(OH)_2$ | 0.95 | 20 | 42 | 2.1 | 1.5 |
| Pt/BaKL | $Ba(NO_3)_2$<br>$Pt(NH_3)_4(OH)_2$ | 4.81<br>1.02 | 13 | 25 | 3.8 | 2.8 |
| Ru/KL | $RuNO(NO_3)_2$ | 2.03 | 60 | 30 | 4.5 | 3.9 |
| Ru/HSAG | $RuNO(NO_3)_2$ | 1.99 | 43 | 22 | 6.0 | 3.7 |

The TPR profiles in Fig. 1 show that the reduction of the catalytic precursors occurs below 623 K, therefore under the reduction treatment employed, typically at 673 K, all catalysts were fully reduced. It should be noted that the TPR measurements of the unloaded zeolites did not showed hydrogen consumption. The profile of Pt/KL exhibits a broad peak between 373 and 580 K centered at 473 K, with a shoulder at 407 K, which substantially agrees with that reported by Ostgard et al.[29] Following these authors the peak at 473 K must include the reduction of PtO and $PtO_2$ species formed during the calcination step. The shoulder at 407 K could be related to the reduction of $Pt^{2+}$ species located on the external surface of the zeolite, that is, in the intercrystalline spaces.[28] The addition of Ba modified the reduction profile (sample Pt/BaKL) causing variations in the relative intensity of the peaks and shifting the maximum reduction rate towards higher temperatures, which is in agreement with previous reported and discussed results.[25] The only reduction peak observed, with a maximum at 523 K is assignable to the reduction of $Pt^{4+}$ or $Pt^{2+}$ to $Pt^0$. Concerning the particle sizes of BaO we have different evidences that this component is well dispersed. Firstly because BaO peaks are not detected in the X-ray diffraction patterns and secondly because the analysis by X-ray energy dispersive spectroscopy, carried out in the TEM equipment, indicates a homogeneous distribution of Ba in the catalyst surface.

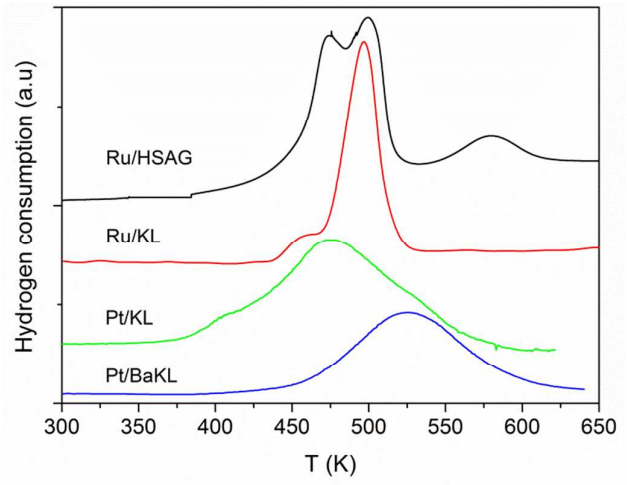


**Fig. 1.** TPR profiles of the catalysts.

On the other hand, the TPR profile of Ru/KL exhibits a peak at 495 K with a shoulder at 460 K. This suggests that the reduction of the ruthenium precursor occurs in two steps. In the first step, $Ru^{3+}$ is reduced to $Ru^{2+}$, while in the second one $Ru^{2+}$ is subsequently reduced to $Ru^{0}$, and also that this reduction profile includes hydrogen consumption of anionic species, taking into account that this catalyst was not subjected to a previous calcination step.[30] For the Ru/HSAG sample, the TPR profile shows in similar manner the reduction in two steps but at slightly higher temperatures, at 474 and 499 K. Another peak observed at 550 K can be related to both hydrogen consumption and methane formation, which at this low temperature is associated with the reduction of oxygen groups on the surface of the graphite support, very probably around the metal particles.[31,32]

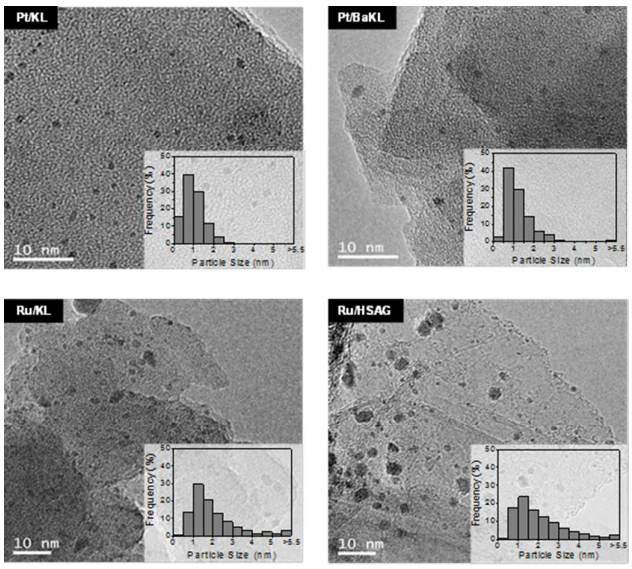


Fig. 2. TEM micrographics and particle size distribution of catalysts.

The TEM data were recollected and normalized obtaining typical distributions of crystallite sizes. As it can be seen in Fig. 2, these samples exhibit a wide distribution of metallic nanoparticles, whose medium particle sizes are quantitatively much smaller than the average particle sizes calculated from the CO chemisorption measurements. The fact that the average sizes of the crystals ($d_{TEM}$) given in Table 1 are larger than the dimensions of the cavities (0.48 x 1.24 x 1.07 nm) and window (0.71 nm) of the zeolite, together with the presence of very small metallic particles, evidenced in the TEM micrographs, suggests a bimodal distribution of the particle size in the zeolite, i.e., metal clusters inside the channels and metal crystals on the external surface, as above suggested. The $d_{TEM}$ values for the Pt catalysts, as well as the data obtained from CO chemisorption, reveal differences between the two platinum catalysts, which are a consequence of the different surface area of the KL and BaKL supports, the higher the surface area the lower the average particle size. On the other hand, the metal average particle size of Ru/KL catalyst is quite larger than that for Pt/KL catalyst. This result could be related to the partial blocking of the pore mouth by Ru particles in Ru/KL, as suggested by the BET surface area (159 $m^2/g$) which is much lower than that measured for Pt/KL (220 $m^2/g$). Besides, in the representative TEM image exposed in Fig. 2 it can be observed a quite heterogeneous distribution with large metal particles together with other smaller one. Study by TEM of the Ru/HSAG sample was also performed and the respective micrographs given in Fig 2. For this sample metal particles of a wide variety of sizes, with average particle size of 3.7 nm, are observed.

### Catalytic behaviour

**Conversion, activities and selectivities.** The catalytic conversions and the corresponding turn-over frequencies (TOF) for all the catalysts, in the pure ethanol decomposition reaction, are displayed in Table 2. Conversion was defined as the percentage of ethanol fed to the reactor transformed into organic products (CO is not considered as discussed below). While TOF is referred to the activity of each metallic surface site per unit time, being the number of surface sites those determined from the CO chemisorption measurements. The two zeolite supports, KL and BaKL, were tested under the reaction conditions, and the conversions obtained were lower than 0.4%. In addition, these zeolite supports gave acetaldehyde as the only reaction product (trace amounts) in accordance with the basic character of both zeolitic materials. This catalytic behavior is clearly different to that reported for acid zeolites[33], i.e. HZSM-5, where the main reaction product is ethylene, but it is in good agreement with the performance reported for ZY and ZSM-5 ion exchanged with alkaline cations.[15]

On the other hand, the TOF values shown in Table 2 demonstrate that surface sites of Pt catalysts are one order of magnitude more active than those of Ru samples. The higher ethanol dehydrogenation activity of Pt nanoparticles can result from the fact that the primary product, acetaldehyde, undergoes conversion via C-C bond splitting of the adsorbed $CH_xCO$ species releasing gaseous CO and $CH_4$ and allowing

further chemisorption and reaction of reactant molecules on the free surfaces sites. Briefly, over Pt catalysts the initially produced acetaldehyde suffers a decarbonylation reaction leaving clean the surface for new ethanol adsorption-reaction processes. Also these differences can be attributed to the intrinsic activity of each metal, and these intrinsic activities can be also influenced by some morphological and geometrical properties of the catalysts, such as size, shape and location of metal particles in the zeolite framework.

The main obtained products are acetaldehyde, produced by dehydrogenation of ethanol; ethylene, produced by dehydration; ethane, likely formed by hydrogenation of ethylene, and methane always along with carbon monoxide. These two latter are products of decarbonylation reactions. As before indicated this decarbonylation reaction gives $CH_4$ and CO in exactly equal amounts, as checked by gas chromatography analysis. Clearly Table 2 shows that while on Pt catalysts the reaction proceeds up to decarbonylation products, Ru ones yield mainly acetaldehyde. Figure 3 shows the product distribution obtained over all catalysts at different temperatures. The reported results are given after 1 h, which correspond to the steady state conditions. For platinum catalysts, the increase of the reaction temperature highly decreases the selectivity towards acetaldehyde in favor of the methane production, this indicating that the activation energy of the acetaldehyde decarbonylation reaction is lower than that of the ethanol dehydrogenation. This modification in the reaction products was also observed during the DRIFTS analyses, as will be indicated in the corresponding section. For Ru catalysts the negative effect of the temperature on the selectivity towards acetaldehyde is much less appreciable, because this is always the predominant product. In this sense formation of methane over Ru/KL was only observed above 523 K of reaction temperature. For Ru/HSAG at the lower temperature (473 K) diethyl ether (DEE) and ethylene were found along the majority acetaldehyde. Although when the reaction temperature increases, the DEE disappears while ethylene and ethane were the by-products favored (Fig. 3). These compounds (DEE and ethylene/ethane) are dehydration products. Considering that the dehydration reaction is catalyzed by acid surface sites, the formation of these products indicates that, in agreement with previous results,[31,34] some acid sites are generated on the carbon support during the preparation of the catalyst with ruthenium (III) nitrosyl nitrate precursor.

Table 2. Activity and selectivity of the catalysts in the ethanol decomposition at 573 K with pure ethanol in the feed.

| Catalyst | X (%) | TOF $10^2$ ($s^{-1}$) | Selectivity (%) | | | |
|---|---|---|---|---|---|---|
| | | | Acetal. | Ethylene | Ethane | Methane |
| Pt/KL | 11.0 | 41.0 | 35 | nd* | nd | 65 |
| Pt/BaKL | 10.0 | 66.0 | 20 | nd | nd | 80 |
| Ru/KL | 6.0 | 2.1 | 90 | nd | nd | 10 |
| Ru/HSAG | 2.7 | 3.9 | 70 | 20 | 10 | 0 |

*nd denotes negligible or no detected amount of this product.

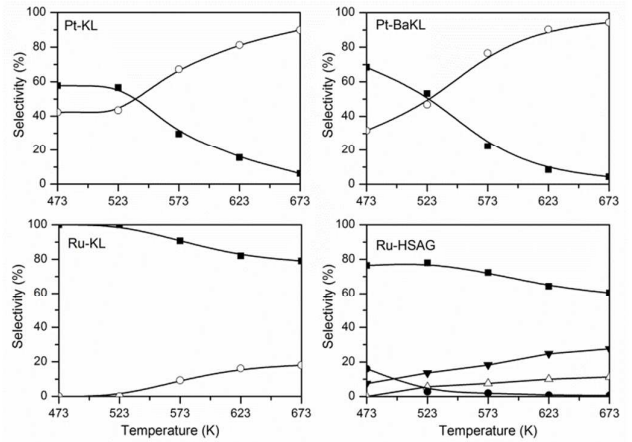


**Fig. 3.** Selectivity towards the main reaction products as a function of the temperature. (■) acetaldehyde, (○) methane, (▼) ethylene, (Δ) ethane, (●) DEE.

**Stability of catalysts and role of water co-feeding on the catalytic properties.** Fig. 4a shows the effect of the time on stream up to 400 min on the performance of the catalysts at 573 K using pure ethanol in the fed. The high catalytic stability observed for Pt-catalysts indicates that neither coke deposition nor sintering phenomena take place on this metal surface. The excellent stability observed for the supported Pt nanoparticles is ascribed to the acetaldehyde decarbonylation reaction, which yields methane and carbon monoxide, and acts removing this primary product from the catalytic surface. In contrast, a significant decrease of catalytic activity is observed for the Ru catalysts. This behavior is particularly evident for the Ru/KL sample, where 30% of activity loss was observed after 380 min on stream. Notice that even if the reaction is maintained under differential conditions this loss of activity is clearly evident. In order to understand the causes of deactivation, a sample of Ru/KL was studied in reaction in two successive runs, with an intermediate treatment under hydrogen flow at 573 K between the first and the second run.
For this Ru/KL sample, it was observed the recovery of the initial activity in the second reaction test and its subsequent decay. This behavior evidences a deposition of carbonaceous species, probably derived from the acetaldehyde interaction (or decomposition of sub-products strongly adsorbed) over the surface of Ru nanoparticles, which are easily removed by hydrogen treatment. Furthermore the higher extension of the deactivation observed over Ru/KL compared with Ru/HSAG (Fig. 4a), both catalysts with similar mean particle sizes (Table 1), indicates that the nature of the support materials may have a significant role in the generation or in the stabilization of these carbon deposits. On the other hand no modifications in the selectivity values were observed with the time on stream during isothermal condition reactions.

Comparing the above catalytic results (Fig. 4a) with those obtained feeding ethanol+water (Fig. 4b), it is noted that in both cases the Pt catalysts are equally stable. Nevertheless, they are less active when water is present in the reactant

mixture. The lower activity (approximately 45%) obtained in the presence of water can be indicating that water competes with ethanol for the adsorption sites on the Pt catalysts. This latter, however, does not modify significantly the product distribution, as evidenced when comparing the selectivity results presented in Tables 2 and 3.

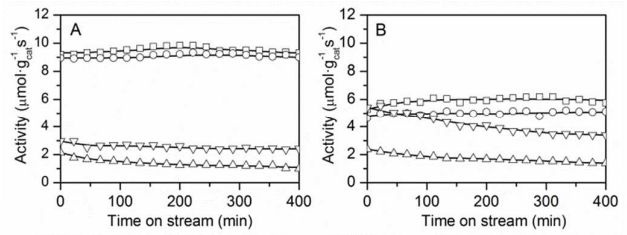


Fig. 4. Stability tests in ethanol decomposition reaction at 573 K with A) ethanol pure flow and B) Ethanol + water (10%) flow for the different catalysts: (□) Pt/KL, (○) Pt/BaKL, (△) Ru/KL, (▽) Ru/HSAG.

In the case of the Ru catalysts the deactivation after 400 min on stream is somewhat higher in the presence of water (41% for Ru/KL and 38% for Ru/HSAG) than in pure ethanol (30% for Ru/KL and 19% for Ru/HSAG). Contrarily to that observed for the Pt catalysts, the Ru catalysts are more active in the ethanol+water reaction mixture, especially in the case of Ru/HSAG for what the TOF goes from 0.039 to 0.110 $s^{-1}$, as reported in Tables 2 and 3. All these findings can be attributed to support effects. With respect to the selectivity patterns, also presented in Tables 2 and 3, Ru/KL behaves similarly to Pt catalysts, since its product distribution is not excessively modified. In the case of Ru/HSAG catalyst some modifications are however observed in the product distribution. Thus, with pure ethanol this catalyst yields minor amounts of ethylene and ethane (Table 2), while in the presence of water-ethanol mixture only ethylene was produced, along with a small amount of methane. Therefore, the dehydration reaction which seems to takes place on acid surface sites of the Ru/HSAG catalyst is reversed (hindered) in the presence of water.

**Table 3**. Activity and selectivity of the catalysts in the ethanol decomposition at 573 K with ethanol+water mixture in the feed.

| Catalyst | X (%) | TOF $10^2$ ($s^{-1}$) | Selectivity (%) | | | |
|---|---|---|---|---|---|---|
| | | | Acetal. | Ethylene | Ethane | Methane |
| Pt/KL | 6.1 | 22.0 | 25 | nd* | nd | 75 |
| Pt/BaKL | 6.5 | 43.0 | 20 | nd | nd | 80 |
| Ru/KL | 8.5 | 3.0 | 80 | nd | nd | 20 |
| Ru/HSAG | 5.8 | 11.0 | 85 | 10 | nd | 5 |

* nd denotes negligible or no detected amount of this product.

**In situ reaction surface species by DRIFTS**

In order to obtain more insight about the nature of the reaction intermediates, separate experiments about ethanol decomposition over Pt/KL, Pt/BaKL and Ru/KL samples, were performed in situ in a DRIFT catalytic chamber. The reaction was studied at various different temperatures in the range 373-723 K. Spectra at each temperature were registered after 10 min where stabilization was achieved. Fig. 5 shows the evolution of recorded spectra. In this figure the IR absorption bands located between 3780 $cm^{-1}$ and 3790 $cm^{-1}$ can be related to the stretching vibrations of OH groups, but these bands are covered by the broad band of the own zeolite. Bands around to 2980 $cm^{-1}$ are characteristic of the presence of strong stretching signals of C-H bonds of ethanol.[35,36] These bands lose intensity with increasing temperature, indicating that the adsorbed amount of ethanol decreases when increasing the temperatures and/or that these adsorbed species are involved in the formation of different surface species and reaction products. Besides the bands associated to ethoxy species (1045, 1084, 1400 and 1450 $cm^{-1}$) and ethanol molecularly adsorbed (1265 $cm^{-1}$),[37,38] it was detected the presence of the band at 1720 $cm^{-1}$. This band at around 1670-1720 $cm^{-1}$ has been attributed to the stretching vibrational mode of CO in acetyl species,[39-41] which are intermediates in the reaction mechanism of the acetaldehyde formation on the metal surfaces.[42] These oxygenated compounds are produced by dehydrogenation of ethoxy species. It is important to notice that the spectra registered for the bare KL zeolite, under reaction conditions, show neither bands associated with the reactant ethanol nor with the dehydrogenation or dehydration products. Thus, these results indicate again the lower catalytic activities of KL basic surface sites in comparison with the metallic surface sites.

Journal Name

ARTICLE

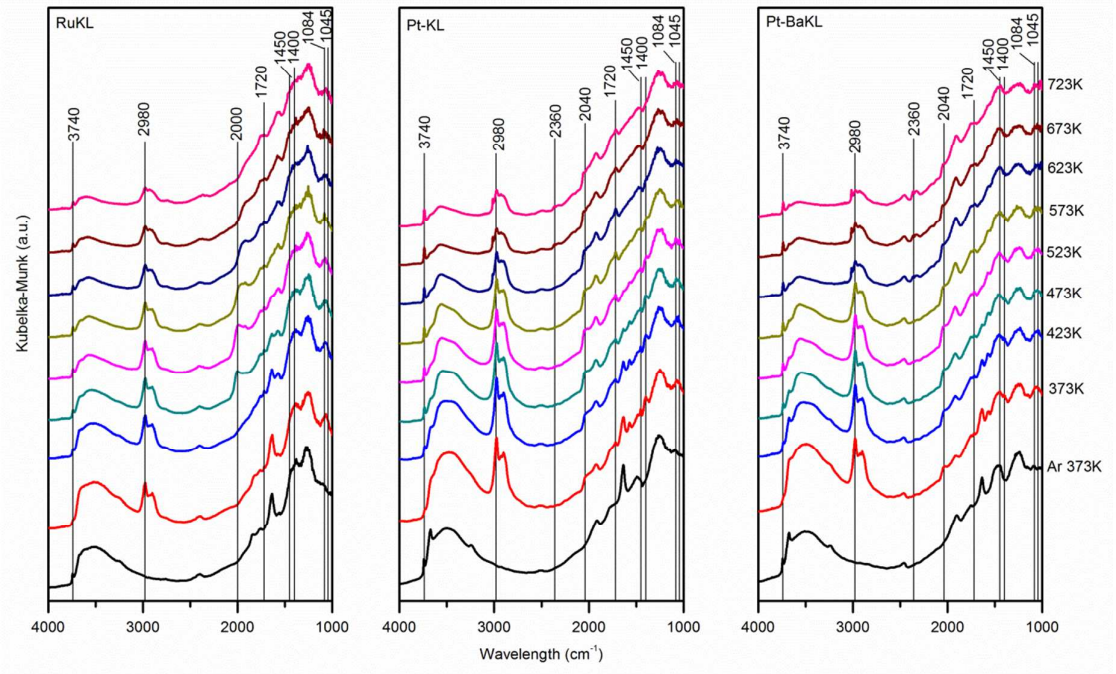


**Fig. 5**. Infrared spectra of the surface species formed by ethanol adsorption on reduced Ru/KL, Pt/KL and Pt/BaKL at different temperatures and spectra of the solids recorded under inert atmosphere at 373K.

.

Small bands between 2000-2045 $cm^{-1}$ are associated to linear CO adsorption on large metallic particles, typically located at the external surface of zeolite.[43,44] Concerning this band, two different trends were observed, depending on the nature of the metal. For Ru/KL catalyst, the intensity of the band reached a maximum at around 523 K, losing its intensity with the increasing temperature, and completely disappearing above 623 K. On the other hand, with platinum catalysts, the intensity of this band increased with the reaction temperature evidencing their higher catalytic activity for acetaldehyde decarbonylation, in agreement with previous steady state reaction results showed in Fig. 3. These results suggest that the acetaldehyde was decomposed into CO, which is in agreement with the studies of McCabe et al.[45-47] Also in the case of platinum catalysts, at reaction temperatures higher than 673 K, it was detected the presence of the bands around 2300-2400 $cm^{-1}$, which were associated to the $CO_2$ formation.[48] The presence of $CO_2$ could be attributed to the Water Gas Shift (WGS) reaction ($CO + H_2O \leftrightarrow CO_2 + H_2$). Concerning the WGS reactant water, as in these experiments pure ethanol was fed (diluted in Ar) and considering the null selectivity of the Pt/KL and Pt/BaKL catalysts towards dehydration reactions (see selectivity values in Table 3), the only possibility is that the water molecules are originated by the desorption of strong adsorbed water inside the internal porosity of the KL zeolite.

**Proposed reaction pathways**

The formation of the different products over the four studied catalysts can be explained with the help of the simplified set of reactions:

$CH_3CH_2OH \rightarrow CH_3CHO + H_2$ (1)

$CH_3CH_2OH \rightarrow CH_2CH_2 + H_2O$ (2)

$CH_3CHO \rightarrow CH_4 + CO$ (3) decarbonylation

$CH_2CH_2 + H_2 \rightarrow CH_3CH_3$ (4) hydrogenation

$CO + 3H_2 \rightarrow CH_4 + H_2O$ (5) methanation

$CO + H_2O \rightarrow CO_2 + H_2$ (6) water gas shift

Acetaldehyde derives from the dehydrogenation of ethanol mainly produced over both metallic (Ru and Pt) surface sites following reaction 1. With Pt catalysts, as before indicated an increase of the reaction temperature (Fig. 3) favored the methane production via reaction 3. Thus, at lower reaction

temperatures it is apparent that dehydrogenation reaction is predominant, but when increasing the temperature decarbonylation process becomes the principal. Therefore carbon monoxide and methane seem to be originated by decarbonylation of acetaldehyde, through C-C bond cleavage.[49-54] The methane produced can also be derived from the CO hydrogenation (reaction 5).

The addition of 5 wt % Ba (Pt/BaKL catalyst) favors the methane production. Since Ba was incorporated into the zeolite by impregnation, it is reasonable to assume that upon calcination at 873 K was mainly transformed into BaO. Furthermore in this sample an electron transfer towards Pt through the interface BaO-Pt could occur, with subsequent electronic enrichment of Pt.[55] Thus, this phenomenon could contribute to the higher decarbonylation activity of this sample, following the reaction (3). For Ru/HSAG catalyst, the presence of acidic sites on the support, generated during the preparation of the catalyst with the Ru ex-nitrosyl nitrate precursor,[34] favors dehydration of ethanol obtaining ethylene and ethane as byproduct (reactions 2 and 4). Obviously, the primary product ethylene, formed from dehydration of ethanol over the acid sites exposed on the carbon support, is subsequently hydrogenated into ethane over the metal sites using the hydrogen arising from dehydrogenation of ethanol. Finally the $CO_2$ formation, only observed in the case of Pt catalysts (see Fig. 5), can be originated by the water-gas shift reaction (6). In the case of Pt catalysts the dehydration of ethanol does not take place, therefore the water reactant in the water-gas shift process stem from the methanation reaction (5).

In general the selectivity towards a given product is different for the four studied catalytic materials (Pt/BaKL, Pt/KL, Ru/KL and Ru/HSAG), and these results evidence that both the nature of the metal and the selected support govern the pathways for this type of reactions.

## Conclusions

Under the experimental conditions used in this study ethanol is mainly transformed to acetaldehyde over the surfaces of the metal nanoparticles, either Ru or Pt. The catalysts supported on the KL zeolite seem to have a monofunctional metallic performance in the reaction, in spite of the basic properties of KL zeolite. However, in the case of the catalyst with the HSAG support the presence of surface acid sites is enough to produce ethylene by dehydration of ethanol. The subsequent hydrogenation of this primary product over Ru particles leads to ethane, probably with some hydrogen species derived from the dehydrogenation reaction. Over Pt nanoparticles the acetaldehyde suffers decarbonylation reaction, yielding methane and carbon monoxide. By this secondary reaction the catalytic surface is freed from the primary product acetaldehyde. As a lateral consequence Pt deactivates less than Ru, probably due to a diminished presence of deposited carbon species.

The presence of water in the reactant feed does not significantly affect the product distribution, but decreased catalytic activities values, more significantly in the case of Ru samples. This may indicate that water competes with ethanol by the same adsorption sites of the metallic surfaces. The hydrophobic character of HSAG in Ru/HSAG catalyst initially leads to an increased catalytic activity in presence of water, but it does not prevent the deactivation during isothermal reaction conditions.

The DRIFTS study of the reactivity of ethanol on the surface of these catalysts reveals a series of intermediates that participate in the reaction mechanisms. So acetaldehyde formation appears in the main pathway. Furthermore in the case of Pt was also observed the formation of CO species, and under some reaction conditions their subsequent transformation to $CO_2$ via Water Gas Shift (WGS) reaction.

## Acknowledgements

Financial support of the Spanish Government by Projects CTQ2011-29272-C04-01 and 03 is recognized. M. Almohalla thanks the Ministerio de Economía y Competitividad for a FPI Predoctoral Fellowship.

## References

1 D. Sebastián, I. Suelves, E. Pastor, R. Moliner and M. J. Lázaro, *Appl. Catal. B: Environ.,* 2013, **132**, 13-21.
2 J. Rass-Hansen, H. Falsig, B. Jørgensen and C.H. Christensen, *J. Chem. Technol. Biotechnol.,* 2007, **82**, 329-333.
3 E.A. El-Katatny, S.A. Halawy, M.A. Mohamed and M.I. Zaki, *Appl. Catal. A: Gen.*, 200, **199**, 83-92.
4 N.R.C.F. Machado, V. Calsavara, N.G.C. Astrath, C.K. Matsuda, A.P. Junior and M.L. Baesso, *Fuel*, 2005, **84**, 2064-2070.
5 V. Calsavara, M.L. Baesso and N.R.C.F. Machado, *Fuel*, 2008, **87**, 1628-1636.
6 M. J. Skinner, E.L. Michor, W. Fan, M. Tsapatsis, A. Bhan and L. D. Schmidt, *ChemSuschem.*, 2011, **4**, 1151-1156.
7 J.M.Vohs and M. A. Barteau, *Surf. Sci.,* 1989, **211**, 590-608.
8 F.W.Chang and W.Y. Ku. *Appl. Catal. A: Gen.,* 2003, **246**, 253-264.
9 G. Centi and R.A. van Santen. Catalysis for Renewables: From Feedstock to Energy Production Wiley-VCH, Weinheim, 2007.
10 M.A. Aramendía, V. Borau, C. Jiménez, J.M. Marinas, A. Porras and F.J. Urbano, *J. Catal.*, 1996, **161**, 829-838.
11 Y. Shinohara, T. Nakajima and S.J. Suzuki, *Mol. Struct. Theochem.,* 1999, **460**, 231-244.
12 M.M. Doheim and H.G. El-Shobaky, *Colloids Surf. A.,* 2002, **204**, 169-174.
13 F.S Ramos, A.M. Duarte de Farias, L.E.P. Borges, J.L. Monteiro, M.A. Fraga, E.F. Sousa-Aguiar and L.G. Appel, *Catal. Today*, 2005, **101**, 39-44.
14 T. Yashima, H. Suzuki and N. Hara, *J. Catal.*, 1974, **33**, 486-492.
15 C. Bezouhanova, Y. Kalvachev and V. Nevona, *J. Mol. Catal.,* 1991, **68**, 295-300.
16 X. Bo-Qing, C. Tian-Xi and L. Song, *React. Kinet. Catal. Lett.,* 1993, **49**, 223-228.
17 H. Inokawa, S. Nishimoto, Y. Kameshima and M. Miyake, *Int. J. Hydrogen Energy,* 2011, **36**, 15195-15202.
18 H. Inokawa, S. Nishimoto, Y. Kameshima and M. Miyake, *Int. J. Hydrogen Energy,* 2010, **35**, 11719-11724.
19 D.W. Breck. Zeolite Molecular Sieves. Structure, Chemistry and Use, Wiley & Sons, New York, (1974), 113.

20 W. Han, A.B. Kooh and R.F. Hicks, *Catal. Lett.,* 1993, **18,** 219-225.
21 E. Iglesia and J.E. Baumgartner, *Stud. Surf. Sci. Catal.,* 1993, **75**, 993-1006.
22 P.V. Menacherry and G.L. Haller, *J. Catal.*, 1998, **177,** 175-188.
23 J. Álvarez-Rodríguez, I. Rodríguez-Ramos, A. Guerrero-Ruiz and A. Arcoya, *Appl. Catal. A: Gen.,* 2009, **366**, 114–121.
24 J. Álvarez-Rodríguez, I. Rodríguez-Ramos, A. Guerrero-Ruiz and A. Arcoya, *Appl. Catal. A: Gen.*, 2011, **401**, 56-64.
25 J.M. Grau, X.L. Seoane and A. Arcoya. *Catal. Lett.,* 2002, **83**, 247-255
26 B. Bachiller-Baeza, I. Rodríguez-Ramos and A. Guerrero-Ruiz, *Langmuir*, 1998, **14**, 3556-3564.
27 T. Narita, H. Miura, K. Sugiyama and T. Matsuda, *J. Catal.*, 1987, **103**, 491-495.
28 J.R. Anderson, in: Structure of Metallic Catalysts, Academic Press, 1975, p. 295.
29 D.J. Ostgard, L. Kustov, K.R. Poeppelmeier and W.M.H. Sachtler, *J. Catal.,* 1992, **133**, 342-357.
30 J. Álvarez-Rodríguez, I. Rodríguez-Ramos, A. Guerrero-Ruíz and A. Arcoya, *Catal. Today*, 2005, **107–108,** 302–309.
31 F.R. García-García, M. Fernández-García, M.A. Newton, I. Rodríguez-Ramos and A. Guerrero-Ruiz, *ChemCatChem*, 2013, **5**, 2446-2452.
32 F. Rodríguez-Reinoso, A. Guerrero-Ruiz, C. Moreno-Castilla, I. Rodríguez-Ramos and J.D. López-González, *Appl. Catal.*, 1986, **23**, 299-307.
33 K. Ramesh, L.M. Hui, Y.F. Han and A. Borgna. *Catal. Commun.*,2009, **10**, 567-571.
34 E. Gallegos-Suárez, M. Pérez-Cadenas, A. Guerrero-Ruiz, I. Rodríguez-Ramos and A. Arcoya, *Appl. Surf. Sci.*, 2013, **287**, 108-116.
35 R.W. McCABE and P.J. Mitchell, *J. Eng. Chem. Prod. Res.*, 1984, **23**, 196-202.
36 R.G. Greenler. *J. Chem. Phys.*, 1962, **37**, 2094-2100.
37 J. Rasko, A. Hancz and A. Erdohelyi, *Appl. Catal. A: Gen.*, 2004, **269**, 13-25.
38 A. Yee, S.J. Morrison and H. Idriss, *J. Catal.*, 1999, **186**, 279-295.
39 H. Idriss, C.Diagne, J.P Hindermann, A. Kiennemann and M. A. Barteau*, J. Catal.*, 1995, **155,** 219-237.
40 R. Shekhar, M.A. Barteau, R. V. Plank and J.M. Vohs, *J. Phys. Chem. B.*, 1997, **101**, 7939-7951.
41 T. Shimanouchi, *National Bureau of Standards*, 1972, **1**, 1-160.
42 M. Mavrikakis and M.A. Barteau, *J. Mol. Catal.*, 1998, **131**, 135-147.
43 C. Bezoukhanova, J. Guidot, D. Barthomeuf, M. Breysse and J.R. Bernard, *J. Chem. Soc., Faraday Trans. I*, 1981, **77**, 1595.
44 L.M. Kustov, D. Ostgard and W.M.H. Sachtler. *Catal. Lett.,* 1991, **9**, 121-126.
45 R.W. McCabe, C.L. DiMaggio and R.J. Madix. *J. Phys. Chem.*, 1985, **89**, 854-861.
46 A. Ciftci, D.A.J.M. Ligthart, P. Pastorino and E.J.M. Hensen, *Appl. Catal. B: Environ.*, 2013, **130**, 325-335.
47 A. Gazsi, T. Bansagi and F. Solymosi, *J. Phys. Chem. C.*, 2011, **115,** 15459-15466.
48 A.M. Silva, L.O.O. Costa, A.P.M.G. Barandas, L.E.P. Borges, L.V. Mattos and F.B. Noronha. *Catal. Today*, 2088, **133** 755-761.
49 P. Ciambelli, V. Palma and A. Ruggiero. *Appl. Catal. B: Environ.*, 2010, **96**, 190-197.
50 J.Y. Siang, C.C. Lee, C.H. Wang, W.T. Wang, C.Y. Deng, C.T. Yeh and C.B. Wang, *Int. J. Hydrogen Energy*, 2010, **35**, 3456-3462.
51 H. Idriss. Platinum Metals Review, 2004, **48**, 105-115.
52 D.A. Morgenstern and J.P. Fornango, *Energy and Fuel*, 2005, **19**, 1708-1716.
53 B. Zhang, W. Cai, Y. Li, Y. Xu and W. Shen, *Int. J. Hydrogen Energy*, 2008, **33,** 4377-4386.
54 S. Ito and K. Tomishige. *Catal. Comm.*, 2010, **12**, 157-160.
55 A.F.F. de Lima, R.C. Colman, F.M.Z. Zotin and L.G. Appel, *Int. J. Hydrogen Energy*, 2010, **35,** 13200-13205.

## Graphical Abstract

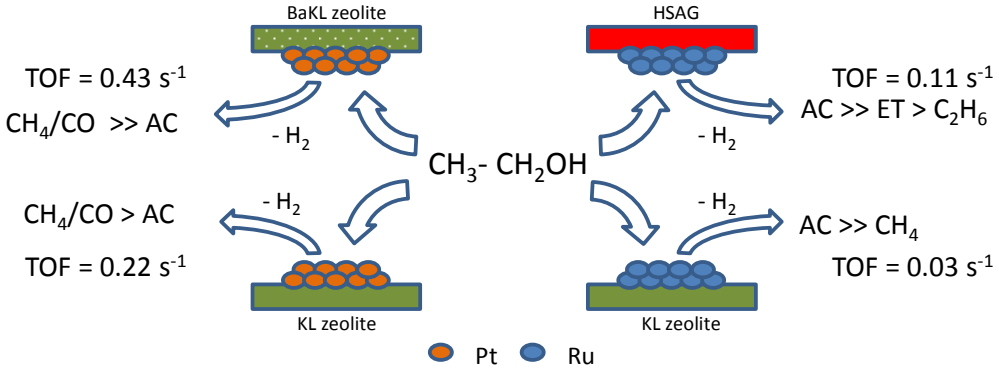


AC – acethaldehyde , ET- ethylene, $CH_4$ – methane, $C_2H_6$ - ethane, CO – carbon monoxide